

Strengthening of Ti_3AlC_2 by incorporation of Si to form $\text{Ti}_3\text{Al}_{1-x}\text{Si}_x\text{C}_2$ solid solutions

Y.C. Zhou*, J.X. Chen, J.Y. Wang

High-performance Ceramic Division, Shenyang National Laboratory for Materials Science, Institute of Metal Research, Chinese Academy of Sciences, 72 Wenhua Road, Shenyang, Liaoning 110016, China

Received 24 March 2005; received in revised form 14 October 2005; accepted 15 October 2005
Available online 27 December 2005

Abstract

A series of $\text{Ti}_3\text{Al}_{1-x}\text{Si}_x\text{C}_2$ ($x \leq 0.25$) solid solutions were synthesized using an in situ hot pressing/solid–liquid reaction method. It was revealed that the lattice parameter c decreased dramatically but a remained almost unchanged with an increase of Si in the $\text{Ti}_3\text{Al}_{1-x}\text{Si}_x\text{C}_2$ solid solutions. A relationship between lattice parameter c (in nm) and Si content x , $c(x) = 1.8541 - (8.5674 \times 10^{-2})x$, was established. A significant strengthening effect was observed when x was greater than 0.15 in the $\text{Ti}_3\text{Al}_{1-x}\text{Si}_x\text{C}_2$ solid solutions: the Vickers hardness, flexural strength and compressive strength were enhanced by 26%, 12% and 29%, respectively, for $\text{Ti}_3\text{Al}_{0.75}\text{Si}_{0.25}\text{C}_2$ solid solution. The electrical resistivities of $\text{Ti}_3\text{Al}_{1-x}\text{Si}_x\text{C}_2$ solid solutions were in the range 0.35–0.37 $\mu\Omega\text{ m}$ and increased slightly with an increase of Si content. The addition of Si to Ti_3AlC_2 to form solid solutions had no deleterious effect on the oxidation resistance at 1100 °C due to the formation of a continuous Al_2O_3 layer.

© 2005 Acta Materialia Inc. Published by Elsevier Ltd. All rights reserved.

Keywords: $\text{Ti}_3\text{Al}_{1-x}\text{Si}_x\text{C}_2$ solid solutions; Strengthening; Electrical resistivity; Oxidation resistance

1. Introduction

Ti_3AlC_2 is one of the most fascinating members of the group of layered ternary compounds called MAX phases, where M is a transition metal, A is a group IIIA or IVA element and X is C or N, due to the unusual combination of the properties that it possesses. The salient properties of this layered ternary ceramic are (other than the merits of good damage tolerance and machinability commonly shared by the ternary carbides of the same family) low density and excellent thermal shock and oxidation resistance [1–3]. Such unique properties make it possible to use Ti_3AlC_2 in structural components for high-temperature applications and as oxidation-resistant coatings on alloy surfaces [4]. However, compared with traditional binary carbides and other layered ternary ceramics such as Ti_3SiC_2 , Ti_3AlC_2 has relatively low hardness and strength,

which limit its range of applications. Thus an improvement in the hardness and strength of Ti_3AlC_2 is necessary to overcome this drawback and widen its range of applications.

Previous work shows that substitutions at the M, A or X sites of MAX phases are all feasible [5–14]. For example, Wang et al. [7] predicted that solid solution strengthening may be operative for $\text{M}_x\text{M}'_{2-x}\text{AlC}$ (M and M' = Ti, V and Cr) solid solutions as the valence electron concentration is in the range 8.4–8.6. Ganguly et al. [8,9] showed the hardness values of $\text{Ti}_3\text{Si}_{1-x}\text{Ge}_x\text{C}_2$ solid solutions were between those of Ti_3SiC_2 and Ti_3GeC_2 . Barsoum et al. [10] reported solid solution hardening in $\text{Ti}_2\text{AlC}_{0.5}\text{N}_{0.5}$ at room temperature, while the solid solution was softer than the end-members, i.e., Ti_2AlC and Ti_2AlN , above 1200 °C.

Based on the results of theoretical and experimental work, it is possible to increase the hardness and strength of Ti_3AlC_2 by alloying or solid solution treatment. It is known that Ti_3SiC_2 is isotypic with Ti_3AlC_2 and Si has one more valence electron than Al. In addition, continuous

* Corresponding author. Tel.: +86 24 23971765; fax: +86 24 23891320.
E-mail address: yczhou@imr.ac.cn (Y.C. Zhou).

solid solutions can be formed in the Ti_3SiC_2 – Ti_3AlC_2 family [15]. Our previous work demonstrated that the mechanical properties of $\text{Ti}_3\text{Si}_{1-x}\text{Al}_x\text{C}_2$ solid solution are similar to those of Ti_3SiC_2 but the oxidation behavior is similar to that of Ti_3AlC_2 [11] when x is greater than 0.1. It is thus expected that strengthening of Ti_3AlC_2 can be achieved by substituting Al in Ti_3AlC_2 with Si to form $\text{Ti}_3\text{Al}_{1-x}\text{Si}_x\text{C}_2$ solid solutions since the valence electron concentration will be increased.

In the present work, we synthesized a series of $\text{Ti}_3\text{Al}_{1-x}\text{Si}_x\text{C}_2$ solid solutions using the well-established in situ hot pressing/solid–liquid reaction method. The change of structural parameters, e.g., lattice parameters, microstructure, with Si content was investigated. The Vickers hardness and flexural and compressive strengths of $\text{Ti}_3\text{Al}_{1-x}\text{Si}_x\text{C}_2$ solid solutions with different Si contents were investigated to demonstrate the strengthening effect. In addition, we measured the electrical resistance and oxidation kinetics of the $\text{Ti}_3\text{Al}_{1-x}\text{Si}_x\text{C}_2$ solid solutions.

2. Experimental

Bulk polycrystalline Ti_3AlC_2 and $\text{Ti}_3\text{Al}_{1-x}\text{Si}_x\text{C}_2$ solid solutions were prepared using the solid–liquid synthesis reaction and simultaneous in situ hot pressing process [16]. In this method, powders of Ti, Al, Si and graphite were used as starting materials. In order to avoid the presence of impurity phases such as TiC and Ti_5Si_3 , the compositions of the initial powder mixtures were optimized. Table 1 lists the compositions of the initial powders for the synthesis of Ti_3AlC_2 and $\text{Ti}_3\text{Al}_{1-x}\text{Si}_x\text{C}_2$ solid solutions with $x = 0.05, 0.10, 0.15, 0.20$ and 0.25 . The powders were weighed and milled in a polypropylene jar for 20 h. After ball milling, the powders were cold pressed into discs of 50 mm in diameter and then put in a graphite die. Solid–liquid reaction synthesis and simultaneous densification were conducted under an Ar atmosphere in a furnace using graphite as the heating element. The synthesis temperature was 1500 °C with a soaking time of 60 min. The final hot pressing pressure was 30 MPa.

The phase composition of the Ti_3AlC_2 and $\text{Ti}_3\text{Al}_{1-x}\text{Si}_x\text{C}_2$ solid solutions was analyzed using X-ray diffraction (XRD). The XRD data were collected using a step-scanning diffractometer with Cu $K\alpha$ radiation (Rigaku D/max-2400, Japan). To identify the change in lattice parameters of Ti_3AlC_2 on addition of Si, nonlinear least squares

fitting using the structure model of Ti_3AlC_2 was performed. The complete profile of the powder diffraction pattern was refined using the Rietveld method [17] employing the DBWS code in the Cerius² computational program for materials research (Molecular Simulation Inc., USA). The intensity is represented by

$$I_{\text{Rietveld}}(2\theta) = b(2\theta) + s \sum_K L_K |F_K|^2 \phi(2\theta_i - 2\theta_K) P_K A_K, \quad (1)$$

where $b(2\theta)$ is the background intensity, s is a scale factor, L_K contains the Lorentz, polarization and multiplicity factors, ϕ is the profile function, P_K is the preferred orientation function, A_K is the absorption factor and F_K is the structure factor. The subscript K represents Miller indices for the Bragg reflections. To measure peak angles accurately, each required peak was scanned with a slow scanning step of 0.02° and was scanned for a time sufficient to acquire adequate intensity.

The Vickers hardness of Ti_3AlC_2 and $\text{Ti}_3\text{Al}_{1-x}\text{Si}_x\text{C}_2$ solid solutions was measured at a load of 10 N with a dwell time of 15 s. Three-point bending tests were conducted to evaluate the flexural strength. The specimens for flexural strength tests were rectangular bars of dimensions $3 \times 4 \times 40 \text{ mm}^3$. The measurements were performed using an electrical universal testing machine at a crosshead speed of 0.5 mm/min. Specimens with dimensions of $2 \times 2 \times 4 \text{ mm}^3$ were cut and ground for compressive tests. The height of a specimen was parallel to the direction of hot pressing. A crosshead speed of 0.5 mm/min was used in compressive testing. The electrical resistance of Ti_3AlC_2 and $\text{Ti}_3\text{Al}_{1-x}\text{Si}_x\text{C}_2$ solid solutions was measured using the standard four-point method. To investigate the oxidation behavior, continuous isothermal mass-change measurements were performed at 1100 °C in air. The samples with different compositions were suspended with a Pt wire in a vertical Setsys 16/18 microbalance (SETARAM, France) and heated at a rate of 40 °C/min to the test temperature. The mass change was recorded continuously as a function of time for up to 200 h.

3. Results and discussion

3.1. Phase composition and microstructure

The XRD patterns of $\text{Ti}_3\text{Al}_{1-x}\text{Si}_x\text{C}_2$ solid solutions with $x = 0$ – 0.25 are shown in Fig. 1. No impurity phases

Table 1
Initial compositions of powders mixtures for Ti_3AlC_2 and $\text{Ti}_3\text{Al}_{1-x}\text{Si}_x\text{C}_2$ solid solutions

Nominal molecular formula	Composition (wt.%)				Stoichiometry Ti:Al:Si:C
	Titanium	Aluminum	Silicon	Carbon	
Ti_3AlC_2	73.69	15.22	0	11.09	3:1.1:0:1.8
$\text{Ti}_3\text{Al}_{0.95}\text{Si}_{0.05}\text{C}_2$	73.53	14.36	0.86	11.25	3:1.04:0.06:1.83
$\text{Ti}_3\text{Al}_{0.90}\text{Si}_{0.10}\text{C}_2$	73.42	13.65	1.58	11.35	3:0.99:0.11:1.85
$\text{Ti}_3\text{Al}_{0.85}\text{Si}_{0.15}\text{C}_2$	73.31	12.80	2.44	11.46	3:0.93:0.17:1.87
$\text{Ti}_3\text{Al}_{0.80}\text{Si}_{0.20}\text{C}_2$	73.15	12.09	3.15	11.62	3:0.88:0.22:1.90
$\text{Ti}_3\text{Al}_{0.75}\text{Si}_{0.25}\text{C}_2$	72.99	4.00	3.40	11.77	3:0.82:0.28:1.93

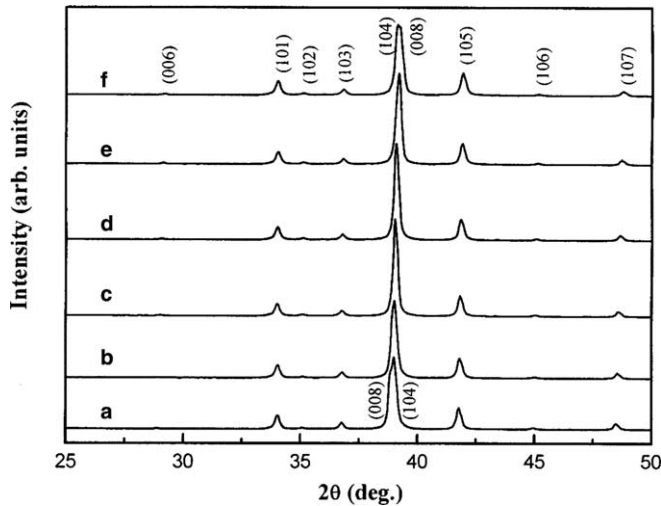


Fig. 1. XRD patterns of $\text{Ti}_3\text{Al}_{1-x}\text{Si}_x\text{C}_2$ solid solutions: (a) $x = 0$, (b) $x = 0.05$, (c) $x = 0.10$, (d) $x = 0.15$, (e) $x = 0.20$, (f) $x = 0.25$.

like TiC , SiC , Ti_5Si_3 and Al_4C_3 were detected within the resolution of the X-ray diffractometer. As shown in Fig. 1, in the whole composition range the phase can be indexed using the structure of Ti_3AlC_2 . Thus we assume that the bulk polycrystalline materials synthesized are single-phase $\text{Ti}_3\text{Al}_{1-x}\text{Si}_x\text{C}_2$ solid solutions, which is consistent with the results of Zhu et al. [14] who added Si to TiC , Ti , Al powder mixtures and prepared impurity-free

Table 2
Rietveld results for Ti_3AlC_2 and $\text{Ti}_3\text{Al}_{1-x}\text{Si}_x\text{C}_2$ solid solutions at 300 K

Nominal molecular formula	Lattice parameters		R-P (%)	R-WP (%)
	a (nm)	c (nm)		
Ti_3AlC_2	0.3072(7)	1.8539(2)	6.6	9.1
$\text{Ti}_3\text{Al}_{0.95}\text{Si}_{0.05}\text{C}_2$	0.3073(1)	1.8496(1)	5.9	8.4
$\text{Ti}_3\text{Al}_{0.90}\text{Si}_{0.10}\text{C}_2$	0.3073(7)	1.8455(5)	5.7	8.6
$\text{Ti}_3\text{Al}_{0.85}\text{Si}_{0.15}\text{C}_2$	0.3073(5)	1.8417(3)	6.9	9.7
$\text{Ti}_3\text{Al}_{0.80}\text{Si}_{0.20}\text{C}_2$	0.3070(9)	1.8371(1)	4.8	7.9
$\text{Ti}_3\text{Al}_{0.75}\text{Si}_{0.25}\text{C}_2$	0.3069(2)	1.8321(7)	6.4	9.3

$\text{Ti}_3\text{Al}_{1-x}\text{Si}_x\text{C}_2$ solid solutions. A careful analysis of the XRD patterns in Fig. 1 indicates that the reflections, especially the (006) and (008) peaks, shift to larger angles with increasing Si content, e.g., the peak position of (008) changes from $2\theta = 38.81^\circ$ for pure Ti_3AlC_2 to $2\theta = 39.24^\circ$ for $\text{Ti}_3\text{Al}_{0.75}\text{Si}_{0.25}\text{C}_2$ solid solution. Interestingly, the peak position of Ti_3AlC_2 (008) shifts from the left to the right side of Ti_3AlC_2 (104), which indicates that the magnitude of lattice parameter c decreases more significantly than that of a .

To describe quantitatively the change of lattice parameters with the amount of Si, Rietveld refinement of the diffraction patterns was performed using Ti_3AlC_2 as the structure model. In all refinements, the reliability factors, i.e., R-P and R-WP values, are less than 10%, as shown in Table 2. The calculated lattice parameters a and c of the $\text{Ti}_3\text{Al}_{1-x}\text{Si}_x\text{C}_2$ solid solutions are plotted as a function of Si content in Fig. 2. It can be seen that as the Si content increases the lattice parameter c decreases dramatically but lattice parameter a remains almost unchanged. A least-squares fit of the lattice parameter c (in nm) yields the expression

$$c(x) = 1.8541 - (8.5674 \times 10^{-2})x \quad (2)$$

where x is the Si content. Extrapolating x to 1, we obtain the lattice parameter c of Ti_3SiC_2 (1.7684 nm). This value is in good agreement with the calculated (1.7670 nm) [18] and measured (1.7671 nm) [15] results.

Fig. 3 shows the microstructures of Ti_3AlC_2 , $\text{Ti}_3\text{Al}_{0.85}\text{Si}_{0.15}\text{C}_2$ and $\text{Ti}_3\text{Al}_{0.75}\text{Si}_{0.25}\text{C}_2$. Comparing the microstructures shown in the figure, it is seen that the average grain size ($\sim 20 \mu\text{m}$) changes very little with the addition of Si.

3.2. Mechanical properties

Fig. 4 shows the measured Vickers hardness versus Si content for the $\text{Ti}_3\text{Al}_{1-x}\text{Si}_x\text{C}_2$ solid solutions, which reveals that the hardness increases slowly for small x but the strengthening effect is significant when x is greater than

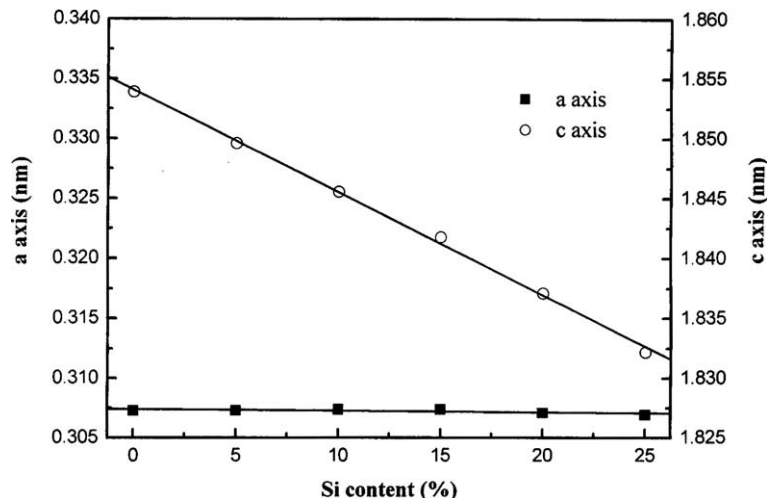


Fig. 2. Lattice parameters of $\text{Ti}_3\text{Al}_{1-x}\text{Si}_x\text{C}_2$ solid solutions calculated from Rietveld refinement using Ti_3AlC_2 as structural model versus Si content.

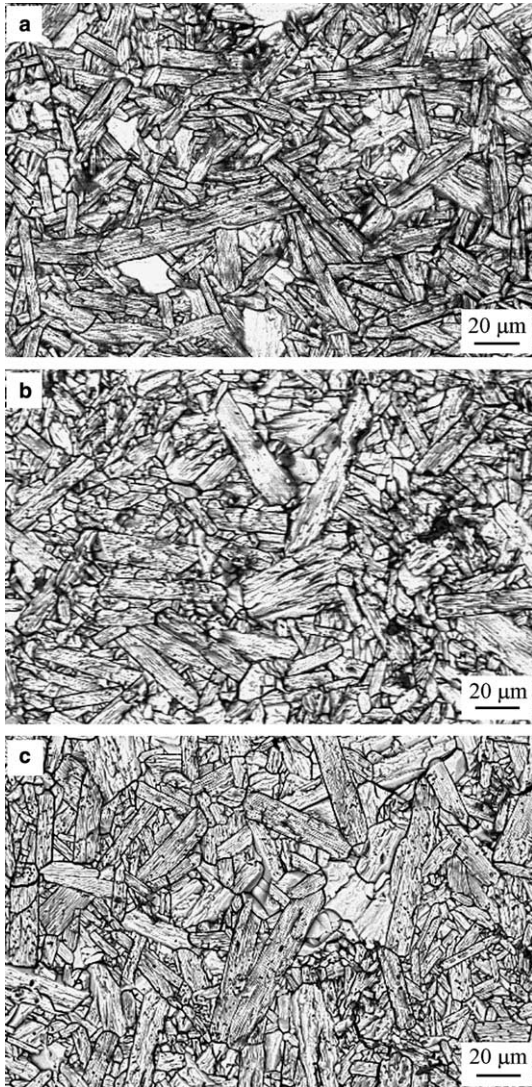


Fig. 3. Microstructure of: (a) Ti_3AlC_2 , (b) $\text{Ti}_3\text{Al}_{0.85}\text{Si}_{0.15}\text{C}_2$ and (c) $\text{Ti}_3\text{Al}_{0.75}\text{Si}_{0.25}\text{C}_2$ solid solutions observed using scanning electron microscopy.

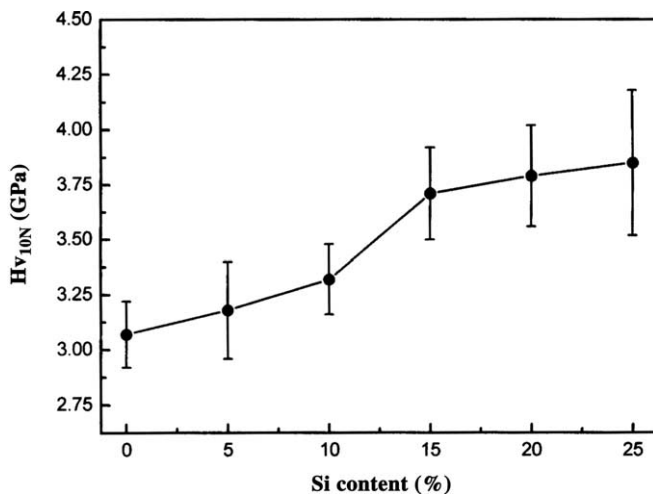


Fig. 4. Measured Vickers hardness of $\text{Ti}_3\text{Al}_{1-x}\text{Si}_x\text{C}_2$ solid solutions as a function of Si content.

0.15. For the $\text{Ti}_3\text{Al}_{0.75}\text{Si}_{0.25}\text{C}_2$ solid solution, the Vickers hardness (~ 3.8 GPa) is enhanced by 26%. However, the value is still lower than that of Ti_3SiC_2 (~ 4.2 GPa). Therefore, like $\text{Ti}_3\text{Si}_{1-x}\text{Ge}_x\text{C}_2$ solid solutions [8], no solid solution strengthening occurs in this system.

A similar strengthening effect can be seen in the strength versus composition curves in Fig. 5, where the flexural and compressive strengths are plotted as a function of Si content. It is noted that when x is greater than 0.15, both flexural and compressive strengths increase demonstrating the significant strengthening effect. When $x = 0.25$, flexural strength and compressive strength are increased by 12% and 29%, respectively.

3.3. Electrical resistivity

The electrical resistivity versus Si content curve is shown in Fig. 6, which shows that the electrical resistivity increases slightly with Si content. Inasmuch as having similar grain size, this change is mainly due to the increase of the electron scatter rate caused by the lattice distortion in the solid solutions. Here the measured electrical resistivities of Ti_3AlC_2 and $\text{Ti}_3\text{Al}_{1-x}\text{Si}_x\text{C}_2$ solid solutions (from ~ 0.35 to ~ 0.37 $\mu\Omega\text{m}$) are slightly higher than that of Ti_3AlC_2 reported previously (~ 0.29 $\mu\Omega\text{m}$) [2], which might result from the difference in microstructure [16], i.e., the samples used here had a finer grain size. This is also consistent with the higher hardness.

3.4. Oxidation behavior

$\text{Ti}_3\text{Al}_{1-x}\text{Si}_x\text{C}_2$ solid solutions display excellent high-temperature oxidation resistance. As an example, Fig. 7 shows the mass gain per unit area ($\Delta W/A$) versus time for $\text{Ti}_3\text{Al}_{0.75}\text{Si}_{0.25}\text{C}_2$ oxidized in air at 1100 °C for up to 200 h. It can be seen that the final mass gain per unit area is only 6.2 g/m^2 .

The oxidation kinetics for $\text{Ti}_3\text{Al}_{0.75}\text{Si}_{0.25}\text{C}_2$ can be roughly divided into two regimes. In the first regime of 0–50 h, the oxidation kinetics nearly obeys a parabolic rate law:

$$(\Delta W/A)^2 = k_p t, \quad (3)$$

where $\Delta W/A$ is the mass gain per unit surface area, k_p is the parabolic rate constant and t is the time. The calculated value of k_p is 1.0×10^{-4} $\text{g}^2 \text{m}^{-4} \text{s}^{-1}$, which is close to that for Ti_3AlC_2 (2.7×10^{-4} $\text{g}^2 \text{m}^{-4} \text{s}^{-1}$) [19] and is much lower than that for Ti_3SiC_2 (4.0×10^{-1} $\text{g}^2 \text{m}^{-4} \text{s}^{-1}$) [20,21].

In the second regime of 50–200 h, however, the mass gain rate slows down and the oxidation kinetics nearly obeys a cubic rate law:

$$(\Delta W/A)^3 = k_c t \quad (4)$$

where k_c is the cubic rate constant and the calculated value is 2.8×10^{-4} $\text{g}^3 \text{m}^{-6} \text{s}^{-1}$.

Hence, the addition of Si into Ti_3AlC_2 to form solid solutions has no deleterious effect on the oxidation resis-

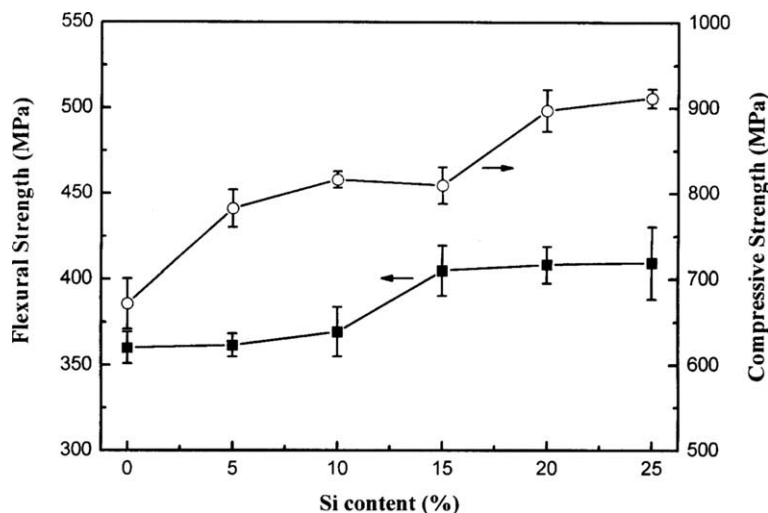


Fig. 5. Flexural and compressive strength of $\text{Ti}_3\text{Al}_{1-x}\text{Si}_x\text{C}_2$ solid solutions as a function of Si content.

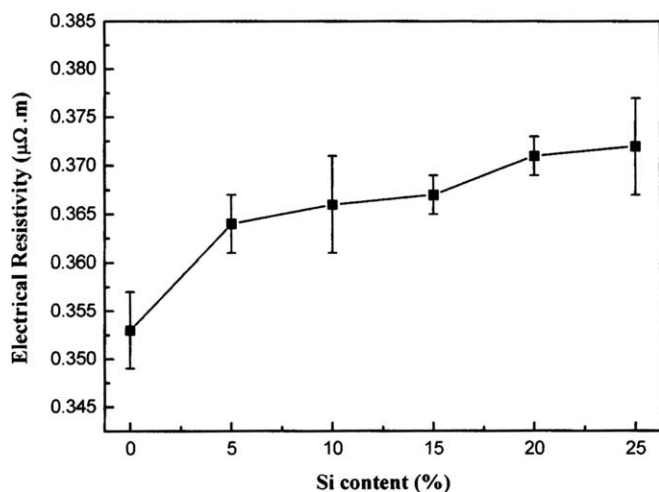


Fig. 6. Measured electrical resistivity versus Si content for the $\text{Ti}_3\text{Al}_{1-x}\text{Si}_x\text{C}_2$ solid solutions.

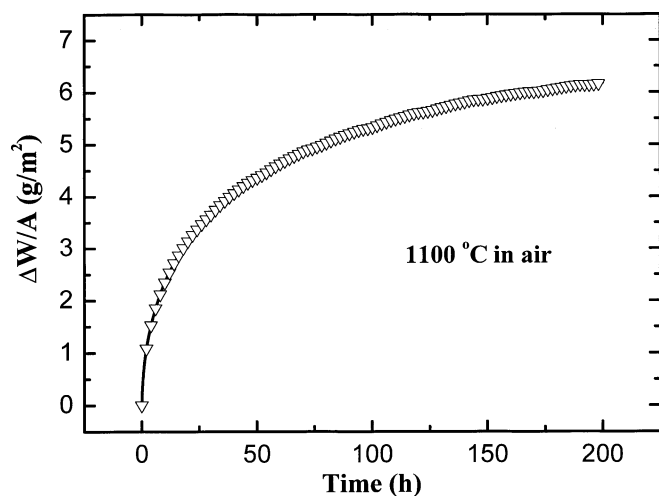


Fig. 7. Mass gain per unit area versus time for $\text{Ti}_3\text{Al}_{0.75}\text{Si}_{0.25}\text{C}_2$ oxidized in air at 1100°C for up to 200 h.

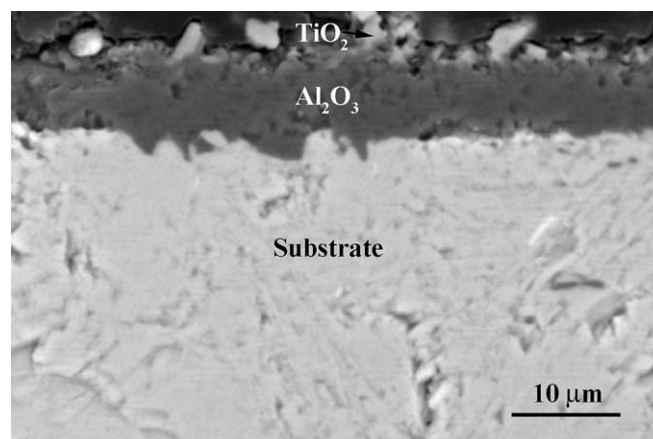


Fig. 8. Backscattered electron image of the polished cross-section of the $\text{Ti}_3\text{Al}_{0.75}\text{Si}_{0.25}\text{C}_2$ solid solution oxidized in air at 1100°C for up to 200 h. Note that the thickness of the oxide layer is only a few micrometers.

tance at this temperature. It is the formation of a continuous inner Al_2O_3 layer (dark) that accounts for the excellent oxidation resistance of the $\text{Ti}_3\text{Al}_{0.75}\text{Si}_{0.25}\text{C}_2$ solid solution, as shown in Fig. 8. After oxidation at 1100°C for 200 h, the thickness of the Al_2O_3 layer is only $7.0 \pm 0.5 \mu\text{m}$. The outer bright phase is discontinuous TiO_2 . The decrease in the mass gain rate during the second oxidation regime might be due to the evaporation of Si by means of forming gaseous SiO . On the interface between the Al_2O_3 layer and the substrate, the oxygen partial pressure is very low, so it is possible that SiO forms and evaporates along the grain boundaries of Al_2O_3 .

4. Conclusion

Ti_3AlC_2 is strengthened by substituting Al with Si to form $\text{Ti}_3\text{Al}_{1-x}\text{Si}_x\text{C}_2$ solid solutions. A significant strengthening effect is observed when x is greater than 0.15 in the $\text{Ti}_3\text{Al}_{1-x}\text{Si}_x\text{C}_2$ solid solutions. The Vickers hardness, flexural

strength and compressive strength of the $\text{Ti}_3\text{Al}_{0.75}\text{Si}_{0.25}\text{C}_2$ solid solution are enhanced by 26%, 12% and 29%, respectively. The electrical resistivities of $\text{Ti}_3\text{Al}_{1-x}\text{Si}_x\text{C}_2$ solid solutions increase slightly with increasing Si content. The addition of Si into Ti_3AlC_2 to form solid solutions has no deleterious effect on the oxidation resistance at 1100 °C.

Acknowledgements

This work was supported by the National Outstanding Young Scientist Foundation for Y.C. Zhou under Grant No. 59925208, and the Natural Sciences Foundation of China under Grant Nos. 50232040, 50302011, 90403027, '863' project.

References

- [1] Tzenov NV, Barsoum MW. *J Am Ceram Soc* 2000;83:825.
- [2] Wang XH, Zhou YC. *Acta Mater* 2002;50:3141.
- [3] Bao YW, Wang XH, Zhang HB, Zhou YC. *J Eur Ceram Soc* [in press].
- [4] Brady MP, Tortorelli PF. *Intermetallics* 2004;12:779.
- [5] Schuster JC, Nowotny H, Vaccaro C. *J Solid State Chem* 1980;32:213.
- [6] Sun ZM, Ahuja R, Schneider JM. *Phys Rev B* 2003;68:224112.
- [7] Wang JY, Zhou YC. *J Phys Condens Matter* 2004;16:2819.
- [8] Ganguly A, Zhen T, Barsoum MW. *J Alloys Compd* 2004;376:287.
- [9] Finkel P, Seaman B, Harrell K, Palma J, Hettinger JP, Lofland SE, et al. *Phys Rev B* 2004;70:085104.
- [10] Barsoum MW, Ali M, El-Raghy T. *Metall Mater Trans* 2000;31A:1857.
- [11] Zhou YC, Zhang HB, Liu MY, Wang JY, Bao YW. *Mater Res Innovat* 2004;8:97.
- [12] Zhang HB, Zhou YC, Bao YW, Li MS. *Acta Mater* 2004;52:3631.
- [13] Salama I, El-Raghy T, Barsoum MW. *J Alloys Compd* 2002;347:271.
- [14] Zhu JQ, Mei BC, Xu XW, Liu J. *Mater Lett* 2004;58:588.
- [15] Barsoum MW. *Prog Solid State Chem* 2000;28:201.
- [16] Wang XH, Zhou YC. *J Mater Chem* 2002;12:455.
- [17] Young RA. Oxford University Press; 1993.
- [18] Zhou YC, Sun ZM, Wang XH, Chen SQ. *J Phys Condens Matter* 2001;13:10001.
- [19] Wang XH, Zhou YC. *Corros Sci* 2003;45:891.
- [20] Sun ZM, Zhou YC, Li MS. *Corros Sci* 2001;43:1095.
- [21] Sun ZM, Zhou YC, Li MS. *Acta Mater* 2001;49:4347.